# High-Throughput Automated Exploration of Phase Growth Kinetics in Quasi-2D Formamidinium Metal Halide Perovskites

Jonghee Yang,[1] Benjamin J. Lawrie,[2,3] Sergei V. Kalinin,[1] Mahshid Ahmadi[1]*

[1] *Institute for Advanced Materials and Manufacturing, Department of Materials Science and Engineering, University of Tennessee, Knoxville, TN 37996, United States*

[2] *The Center for Nanophase Materials Sciences, Oak Ridge National Laboratory, Oak Ridge, TN 37831, United States*

[3] *Materials Science and Technology Division, Oak Ridge National Laboratory, Oak Ridge, TN 37831, United States*

* E-mail: mahmadi3@utk.edu

**Abstract**

Quasi-two-dimensional (2D) metal halide perovskites (MHPs) are an emerging material platform for sustainable functional optoelectronics, however the uncontrollable, broad phase distribution remains a critical challenge for applications. This is because the basic principles for controlling multiple phases in quasi-2D MHPs remain poorly understood, due to the rapid crystallization kinetics during the conventional thin-film fabrication process. Herein, a high-throughput automated synthesis-characterization-analysis workflow is implemented to accelerate material exploration in formamidinium (FA)-based quasi-2D MHP compositional space, revealing the early-stage phase growth kinetics which fundamentally determines the phase distributions. We observe that the prominent *n*=2 2D phase restricts the growth kinetics of 3D-like phases – α-$FAPbI_3$ MHPs where the spacers are coordinated to the surface. δ-$FAPbI_3$ phase further inhibits the growth of 3D-like phases. It is found that thermal annealing is a critical step for proper phase growth, although it can lead to the emergence of unwanted local $PbI_2$ crystallites. Additionally, fundamental insights into the precursor chemistry associated with spacer-solvent interaction that determines the morphologies and microstructures of quasi-2D MHP films are demonstrated. Our high-throughput study provides comprehensive insights into the fundamental principles in quasi-2D MHP phase control and enables new control of the functionalities of complex materials systems for sustainable device applications.

## Introduction

Metal halide perovskites (MHPs) have gained significant attention as materials for high-performance optoelectronic applications due to their favorable optoelectronic properties. The power conversion efficiency of photovoltaics (PVs) based on MHPs has reached up to ~25.8%[1] and green and red light-emitting devices (LEDs) based on MHPs have demonstrated emission efficiencies exceeding 20%.[2, 3] However, one of the major challenges hindering the widespread adoption of MHPs is their instability, which affects the long-term operation and durability of devices.[4, 5] Quasi-two-dimensional (2D) MHPs have recently garnered attention for their unique properties distinctive from those observed in three-dimensional (3D) MHP systems. Quasi-2D MHPs are represented by the chemical formula $L_2A_{n-1}B_nX_{3n+1}$, where L, A, B, and X represent the spacer cations confining the inorganic 2D lattices, monovalent organic/inorganic cations, divalent metal cations, and halides, respectively.[6-8]

Control over the thickness of the $[PbX_6]^{4-}$ octahedra unit in quasi-2D MHPs, denoted by *n*, manifests tunable bandgap and exciton binding energy in a quantum-well electronic structure, beneficial for LED applications.[3, 6, 9-13] Furthermore, quasi-2D MHPs offer improved phase stability compared to 3D MHPs due to the surface-protecting ability of spacer cations against external stresses. Particularly, the implementation of the quasi-2D structure into the long-range 3D MHP lattices that forms '3D-like phases' – a structure of 3D MHP lattice where the spacers are coordinated to the surface – leads to stability enhancement of MHP optoelectronics without compromising the band gap and performances.[13-15]

A major challenge in the development of quasi-2D MHP systems is the difficulty in obtaining a pure desired phase, as multiple phases are often formed during film fabrication.[16] Several efforts were attempted to regulate the multi-phase emergence via spacer engineering,[17] optimal 2D:3D MHP ratio,[13] and additive engineering.[3] Recently, implementation of high-throughput

robotic synthesis platforms have opened a new avenue of materials explorations and processing optimizations,[18] not only accelerating the discovery of functional MHP compositions (particularly in 3D system) but also provides comprehensive insights into the phase distributions, physical properties and stability of the complex quasi-2D MHP systems.[19-21]

Nevertheless, all those strategies have exhibited limited success, which could be attributed to a lack in understanding of the phase growth behaviors of the complex quasi-2D MHP system. It has been shown that the broad phase distribution in quasi-2D MHP stems from the disproportionation of a kinetically-grown intermediate-*n* 2D phase.[17] Still, the understanding of early-stage formation and growth kinetics of quasi-2D MHP phases, primarily determining the phase distribution in the system before disproportionation, remains far elusive. The missing piece originates from the difficulty in capturing the features during the practical film fabrications such as spin-coating, which quickly takes place within a few seconds by solvent evaporation.

Herein, we systematically investigate the phase formation and growth kinetics of quasi-2D MHPs as a function of 2D:3D ratios via high-throughput synthesis and characterization of the microcrystals from the precursor solution, allowing for monitoring the early-stage phase evolution over time.[22, 23] Utilizing an integrated workflow based on high-throughput automated synthesis by pipetting robot, temporal photoluminescence (PL) characterization, and automated peak analysis, comprehensive phase growth kinetics in quasi-2D systems are explored.[22, 23] Formamidinium (FA) and phenethylammonium (PEA) cations are selected as building blocks for the 3D and 2D MHP systems, respectively, due to the excellent performances of the 3D FA MHP optoelectronics,[1, 5] and it is well known that the incorporation of 2D PEA MHPs improves the stability of the entire system.[13]

We found that, unlike the broad phase distributions in methylammonium (MA)- or cesium

(Cs)-based systems,[24] in the FA-based system, up to 95% of 3D $FAPbI_3$ ratio in a compositional space, the *n*=2 2D MHP is the most dominant and stable phase. Higher-*n* (*n*≥5) phases also develop alongside the *n*=2 phase with increasing the ratio of 3D MHP. However, the 3D-like MHPs only appear after the *n*=2 phase has been depleted (beyond 96% $FAPbI_3$ composition ratio). Note that these trends in the large quasi-2D compositional space are further confirmed by the unsupervised machine learning (ML) analysis of the PL spectra.

Characterizations of thin films further reveal that the emergence of the δ-$FAPbI_3$ phase – a room temperature stable non-perovskite phase – particularly at high 3D ratios[25, 26] inhibits the growth of 3D-like phases. Thermal annealing of the films converts the 2D phases to higher-*n* polymorphs, thereby leading to the appearance of 3D-like MHPs. Using hyperspectral cathodoluminescence (CL) microscopy, we reveal that thermal annealing results in formation of local $PbI_2$ crystallite byproduct, which may negatively impact the optoelectronic properties of the quasi-2D MHPs.[27] In addition, we found that the selection of solvent crucially impact on the surface morphologies, microstructures, and local phase inhomogeneities of the quasi-2D MHP films. Chemical principles associated with these features are proposed.

Our study exemplifies how a high-throughput synthesis platform can effectively accelerate our understanding of complex material systems with multiple functionalities. It provides comprehensive insights into the phase growth kinetics of the quasi-2D MHPs and identifies crucial factors that should be considered when designing the formation mechanism of functional semiconductor systems.

## Results and Discussion

### High-throughput exploration of phase evolution kinetics in PEA-FA quasi-2D MHPs

Multiple phases associated with the quasi-2D MHP start to be crystalized from the precursor

solution in a reservoir, in which the synthesized microcrystals undergo dynamic evolutions over time, without leaving kinetically-grown intermediates by solvent evaporation. This allows to *comprehensively elucidate the early-stage phase growth kinetics of the quasi-2D MHP system, which cannot be deeply observed in thin-film fabrication process*. We investigate the phase formation kinetics and evolution of 95 different quasi-2D MHP configurations by varying the 2D:3D precursor ratios in each precursor solution. We use our established automated high-throughput workflow,[22, 23] which includes a robot-based synthesis platform, rapid photoluminescence (PL) characterization, and automated data analysis. The overall methodology is depicted in **Figure 1,** accelerating materials exploration process.

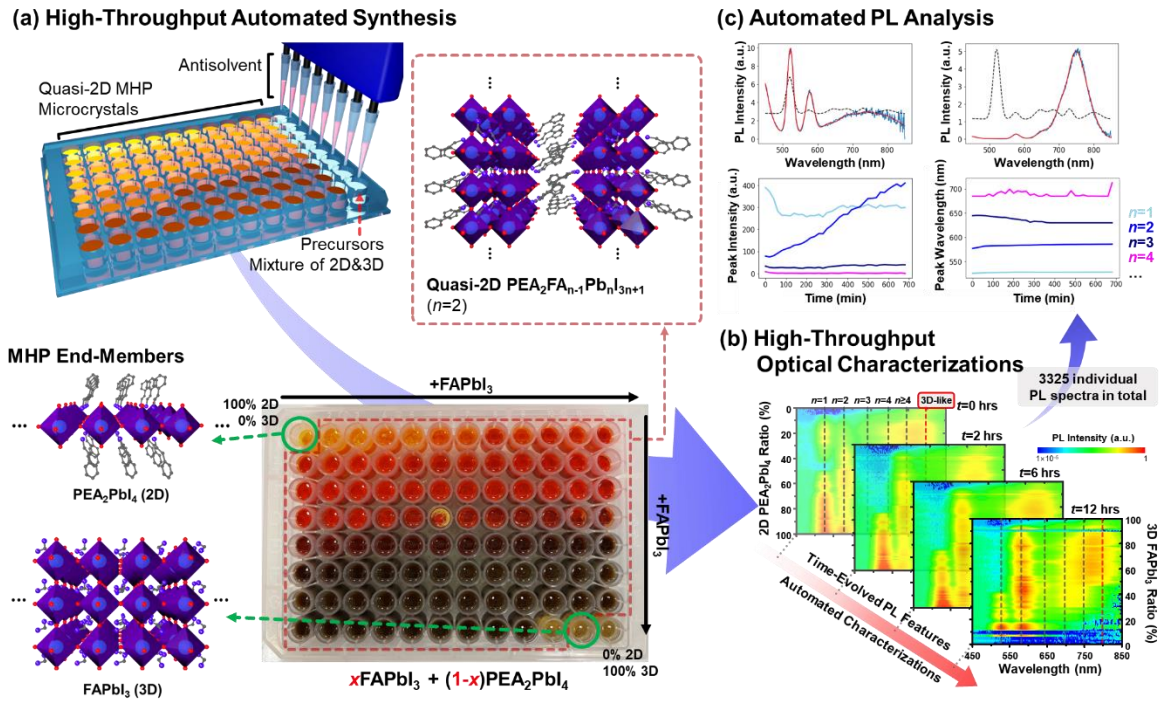


**Figure 1.** (a) Experimental workflow illustrating the automated high-throughput exploration of phase growth in quasi-2D MHPs, with 95 different binary mixtures of 2D $PEA_2PbI_4$ and 3D $FAPbI_3$ end-members. (b) High-throughput PL characterizations for 12 hrs. (c) Implementation of automated peak analysis protocol in the resulting 3325 individual PL spectra to monitor the kinetics of phase formation in each quasi-2D MHP system.

We designed a binary quasi-2D MHP system composed of 2D $PEA_2PbI_4$ and 3D $FAPbI_3$ end-members. Precursor solutions were prepared in a wellplate and crystallized by injecting chloroform as an antisolvent (**Figure 1a**).[12] The resulting wellplate, containing multiple phases of quasi-2D MHP, was then characterized using a high-throughput fast optical reader, enabling monitoring of temporal PL changes and phase evolutions in the quasi-2D system (**Figure 1b**). **Figure S1** shows PL spectra of 95 quasi-2D MHP microcrystal systems collected over 12 hours. To analyze the large PL dataset, an automated peak fitting and tracking protocol was implemented (**Figure 1c)**. This allows for efficient analysis of PL peaks, quantifying intensity and peak center wavelength, with each peak associated with the corresponding 2D and 3D MHP phases. The growth kinetics of each phase in the compositional space of the quasi-2D system were traced by identifying peaks in 3325 individual spectra (95 wells in a plate × 35 PL spectra acquired over a 12-hour period with 20 min intervals). The analysis of the complete dataset only took 5 hours in total.

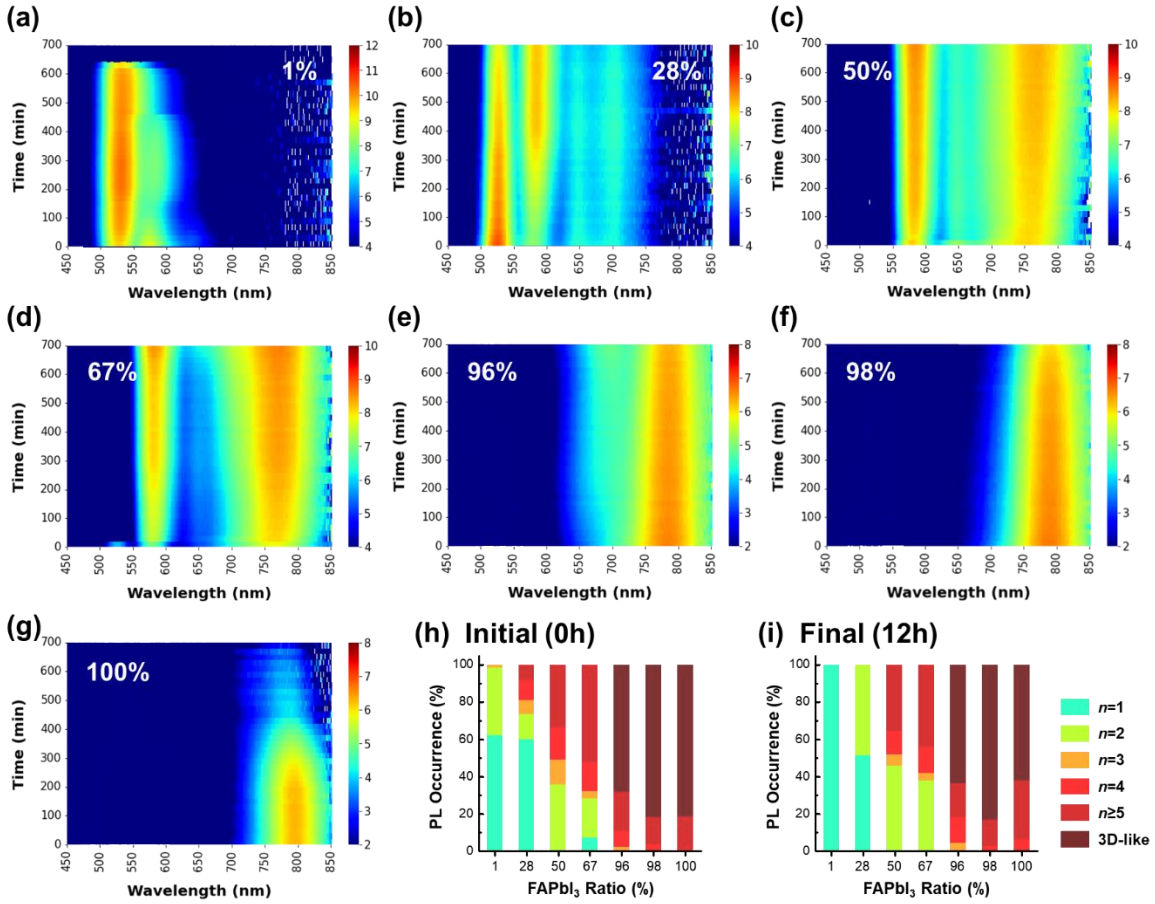


**Figure 2.** (a-g) Time-evolved PL spectra (for ~12 hrs) of quasi-2D MHP microcrystals with key 3D composition ratios from 1 to 100%. The ratio of quasi-2D *n* phases in the microcrystal system, estimated from the corresponding PL peaks of each spectrum at the (h) initial and (i) final (after 12 hrs) timepoints.

The time-evolved PL spectra of selected 2D:3D ratios in 95 binary quasi-2D MHP systems are shown in **Figure 2a-2g**. The relative ratios of each 2D phase, as determined by the relative PL intensity at the initial and final timepoints, are summarized in **Figure 2h and 2i**. For the MHP microcrystals with an exact *n*=1 phase stoichiometry (i.e., $PEA_2PbI_4$), the growth of the MHP phase reaches saturation after a 2.5-fold increase in PL intensity, which is accompanied by a continuous redshift of the PL peak position from 531.5 to around 535 nm (**Figure S2**). This redshift can be attributed to a longer-range stacking of the 2D sheets or horizontal sheet growth, assuming that the increase in PL intensity is proportional to the quantity of synthesized 2D

MHP lattices in an ensemble.

In the microcrystals with a 1% 3D ratio (**Figure 2a**), an initial blueshifted *n*=1 PL peak appears at 527 nm (**Figure S3**). This shift is due to a lower degree of 2D stacking, as evidenced by the lower PL intensity compared to pure 2D. Additionally, an *n*=2 PL peak (centered at ~580 nm) is observed initially, but it disappears over the course of the time series. There is also a weak PL trace reaching ~650 nm which originates from a small amount of *n*=3 2D phase, but it disappears within 100 min. These observations suggest that the introduction of a small amount of 3D component results in the formation of multiple 2D phases as kinetic products, but only the *n*=1 phase remains for a longer time. However, the *n*=1 phase of the microcrystals subsequently disappears after 10 hours by re-dissolution of microcrystals into the precursor state, which is not observed in pure 2D microcrystal system (**Figure S2**). The disappearance of the *n*=1 phase is observed in the microcrystal system with small 3D ratios (up to 11%), particularly where the *n*=2 PL intensity decreases over time. This suggests that insufficient addition of 3D precursors (particularly FA ions) may result in decomposition of the 2D MHPs including *n*=1 phase into its precursor state. The chemical equilibrium of ion-diffusion between the lattice interior and precursor solution – through defects, layer edges and so on – could be associated with the distinct instability of the *n*=1 phases.[17]

With increasing the 3D MHP ratio up to 28%, a noticeable tradeoff in the spectra between the *n*=1 and *n*=2 PL bands is observed (**Figure 2b and S4**). The emergence of the *n*=2 phase becomes more pronounced as the 3D ratio increases (**Figure S5** for 34% 3D ratio). At 50% 3D MHP, the *n*=1 PL becomes negligible (**Figure 2c and S6**). Meanwhile, the changes in PL intensity of *n*=3 and 4 phases (centered at ~640 and ~690 nm, respectively) are insignificant. These results suggest a transition process from the *n*=1 to *n*=2 2D phase driven by the decomposition of the unstable *n*=1 phase, which is *irrespective to the disproportionation of*

*n=3 and 4 phases*. Even at a 95% 3D MHP ratio, the *n*=2 PL emission is still present (**Figure S7**). The *n*=4 phase (centered at ~680-690 nm) is also observed with increasing 3D ratio, but its PL intensity decreases with increasing 3D ratio.

The A-cation site in the quasi-2D MHP lattice can be occupied by either FA or PEA. The rapid crystallization caused by antisolvent injection leads to the formation of multiple phases in the quasi-2D microcrystal system. Density-functional theory (DFT) calculations have proposed that the formation energy of quasi-2D phases increases (i.e., formation becomes difficult) with increasing *n*, with *n*=1 being the easiest phase to form.[28, 29] This is supported by the initial strong *n*=1 PL emission. The absorption spectra of solvated forms of $PbI_2$ in the precursor solution (in γ-butyrolactone; GBL) are consistent for all PEA:FA ratios (**Figure S8**),[30-32] suggesting that the MHP formation reaction is independent of the precursor ratio. Over time, dynamic transformations of these quasi-2D phases result in a reorganization mainly into the *n*=2 phase. This suggests that the phase stability favors *n=2 as the most stable and preferred phase in the mixed ensemble system*. Note that the phase reorganization towards *n*=2 phase takes place above a certain 3D precursor ratio (experimentally ~12%), where the sufficient FA ions are supplied to maintain the phase within the chemical equilibrium of the system.[33]

As the 3D MHP ratio increases, the PL band associated with $n \geq 5$ phases appears and becomes stronger over time, as seen in the microcrystals with 34% 3D MHP (**Figure S5**). At 50% 3D MHP, the intensity of this PL band is comparable to that of *n*=2 (**Figure 2c and S6**); this trend continues up to the 3D ratio of 67% (**Figure 2d**). As the 3D ratio increases to 96%, the emission sharpens and redshifts while the *n*=2 PL disappears (**Figure 2e, S9 and S10**). This suggests that the 3D-like MHP can only be obtained once the formation of the *n*=2 phase is depleted, which can only be observed at high 3D composition ratios (i.e., over 96%). *The growth kinetics of the n=2 phase could obstruct the growth of the 3D-like MHP phase*. Despite that, the stability

of the 3D-like phase is not perfect, disintegrated to lower-*n* phases (e.g., *n*=4) over time.

A distinct PL peak is observed from the 98% 3D MHP microcrystal (**Figure 2f**), with a slight blueshift (~789 nm) from that of pure $FAPbI_3$ (~796 nm; **Figure 2g and S11**). This indicates that at this ratio, the α-$FAPbI_3$ phase dominates the system. However, α-$FAPbI_3$ is not thermodynamically stable at room temperature.[25] The PL of the 3D phase decreases by ~30% after 12 hours, while the PL of pure $FAPbI_3$ completely disappears within 7 hours. These observations are consistent with previous reports in the thin film system, where the PEA spacer passivates the 3D MHP surface and protects the lattice against external stresses.[4, 13]

Overall, high-throughput exploration of quasi-2D MHP compositional space uncovers the early-stage phase formation and growth kinetics in solution phase, which could not be properly observed from device-level or even in-situ film characterizations. We reveal that, among the multiple quasi-2D phases, *n*=2 MHP is the most stable phase and preferentially formed at the early-stage of MHP crystallization. Furthermore, the growth kinetics of *n*=2 phases dominates the quasi-2D MHP compositional space, leaving broad distributions of higher-*n* ($n \geq 5$) phases irrespective to disproportionation of the intermediate phases and suppressing the growth of the 3D-like phase. This not only manifests the energetic disorder in the system but also restricts the growth of the functional 3D-like phases, both limiting the optoelectronic performances – particularly in PV applications.[34]

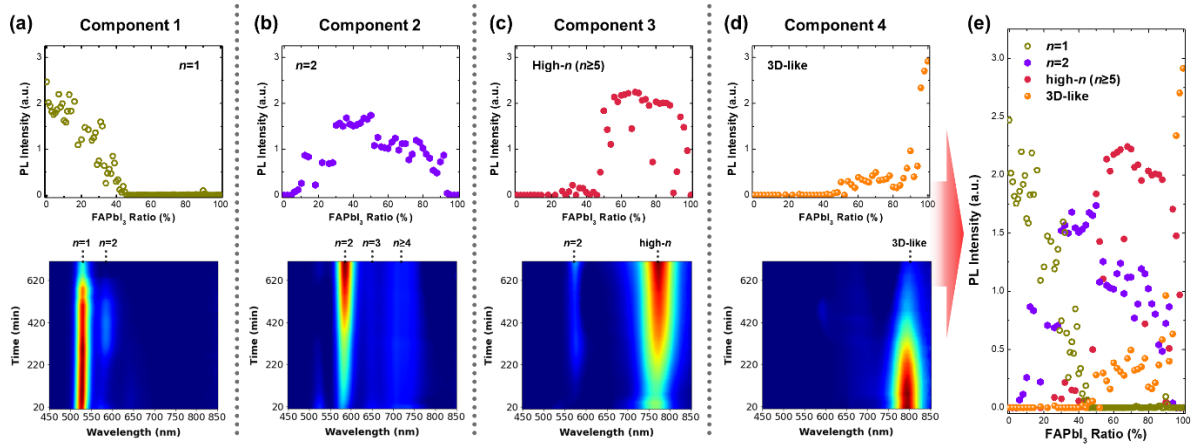


**Figure 3.** (a-d) PL loading maps and the characteristic spectro-temporal PL profiles of each NMF component – illustrating the emergence of each phase in quasi-2D MHPs: (a) $n$=1, (b) $n$=2, (c) high-$n$ ($n$≥5) and (d) 3D-like phase, respectively. (e) Combined the corresponding PL loading maps of four key components in PEA-FA quasi-2D MHP systems by NMF deconvolution.

Multivariate analysis using non-negative matrix factorization (NMF) was applied to analyze the PL data of the quasi-2D MHP system.[23] This method allows for the extraction of key dynamics related to phase growth kinetics and the mapping of time- and composition-dependent PL evolution in the system. Four components were optimally chosen from the analysis: $n$=1, $n$=2, high-$n$ ($n$≥5, PL peak wavelength <~780 nm), and 3D-like (PL peak >780 nm), as shown in **Figure 3a-d**. As can be seen in the analysis, as the 3D ratio increases, the intensity of the $n$=1 phase decreases and eventually disappears at a 3D ratio of around 50% (**Figure 3a**). In contrast, the $n$=2 phase emerges throughout all 3D compositions (**Figure 3b**). The high-$n$ ($n$≥5) phases, accompanied by the $n$=2 phase, develops from the 3D ratio of 50%, but rapidly decreases in intensity at a high 3D ratio of around 94% (**Figure 3c**), where 3D-like phase starts to emerge (**Figure 3d**). The combined loading maps in **Figure 3e** clearly show the general trends in phase distribution in the quasi-2D compositional space, consistent with those observed in the automated workflow. This unsupervised machine learning approach confirms

the overall behaviors of the studied quasi-2D system with the observations made through automated peak fitting, emphasizing its usefulness in the data analysis of high-throughput experiments.

**Emerging features of quasi-2D MHPs in thin films**

To further explore how the initially determined quasi-2D phases at the early-stage of crystallization evolve during film fabrication process, phase evolutions of quasi-2D MHPs in thin films are investigated. Based on our high-throughput synthesis, we selected 6 ratios of 2D:3D, prepared them as thin films using the same conditions (**Figure S12a**), and similarly studied the evolution of PL behavior. The PL results show that the *n*=2 phase is present in the films up to 50% 3D ratios while the *n*=1 is absent. Even in the film with 67% 3D ratio, the *n*=2 phase remains, which is confirmed by the corresponding XRD patterns and absorption spectrum (**Figure S13 and S14**). Note that, for this film, the *n*=2 phase cannot be seen from the PL spectra (**Figure S12e**), attributed to energy transfer to the vicinal higher-*n* phase,[3, 9-12] Meanwhile, the high-*n* (*n*≥5) phases emerge in the films with 3D ratio over 50%, where the corresponding PL band gradually broadened or redshifted over time, likely attributed to the disproportionation of *n*=3~4 phases upon film drying. Note that the overall phase constitutions are analogous to those observed in the microcrystal system, indicating the major phases in the films are primarily determined at the early-stage of phase formation. The use of molecularly tailored spacers and associated organic-inorganic interaction could control the early-stage phase growth kinetics,[17] thereby beneficial to achieve phase-pure quasi-2D system.

In contrast to the microcrystals in the solution phase, thermal annealing was found to be necessary for the formation of higher-*n* and 3D-like phases in the thin films (**Supplementary Note 1**, **Figure S12-14**). This was likely due to the formation of the δ-$FAPbI_3$ phase at room

temperature,[25, 35] which impedes the formation of the 3D-like phase – a structure of α-$FAPbI_3$ MHP lattice where the spacers are coordinated to the surface. X-ray diffraction (XRD) patterns of the films show no appreciable peaks associated with the solvent-intermediate phase (**Figure S14a**),[36] ruling out the influence of the solvent on MHP crystallization. Additionally, thermal annealing induces disproportionation of intermediate phases that results in higher-*n* phases,[17] at the expense of emergence of *n*=1 (for 1% and 28% 3D ratio) or *n*=2 (for 50% and 67% 3D raio) phases.

Local phase inhomogeneities in the quasi-2D MHP films were explored using hyperspectral CL microscopy (**Supplementary Note 2, Figure S15-17**).[37] The CL maps of 2D MHPs are strongly homogeneous. However, it is observed that local $PbI_2$ crystallites emerge on the surface of quasi 2D MHPs after annealing. These results indicate that thermal annealing is necessary for the formation of functional 3D-like α-$FAPbI_3$ phase, but it also results in the emergence of local $PbI_2$ crystallites, which may negatively impact device performance.[27, 37] Given that the pure $PEA_2PbI_4$ is stable up to 250 $^oC$,[38] the incomplete evaporation of solvent in the film before annealing may support thermal disproportionation and decomposition of the lower-*n* phases. Some of the disintegrated ions may be diffused into the higher-*n* lattice, induce ripening of the 3D-like phase[39] or passivate internal defects that results in temporal PL enhancements – observed from the films with 92 and 98% 3D ratios. Meanwhile, the remainder left as $PbI_2$ (and/or δ-$FAPbI_3$) byproducts.

**Figure 4** provides a general schematic of the fate of associated phases in the quasi-2D MHP, offering a comprehensive guide for designing the functional system. Before annealing, the phase distributions in the films are majorly defined at the early-stage of growth process, as observed in microcrystal systems. At high 3D ratios, thermodynamically stable δ-$FAPbI_3$ emerges and suppresses the growth of 3D-like phase. Thermal annealing enables them to

transform to the 3D-like phase and improves crystallinity. However, it also induces lattice disproportionation, which not only results in higher-*n* phases at the expense of intermediate *n*=2-4 phases but also leaves local $PbI_2$ byproducts. The resulting broader phase distributions and the impurity phases can limit the optoelectronic performances.[27, 37]

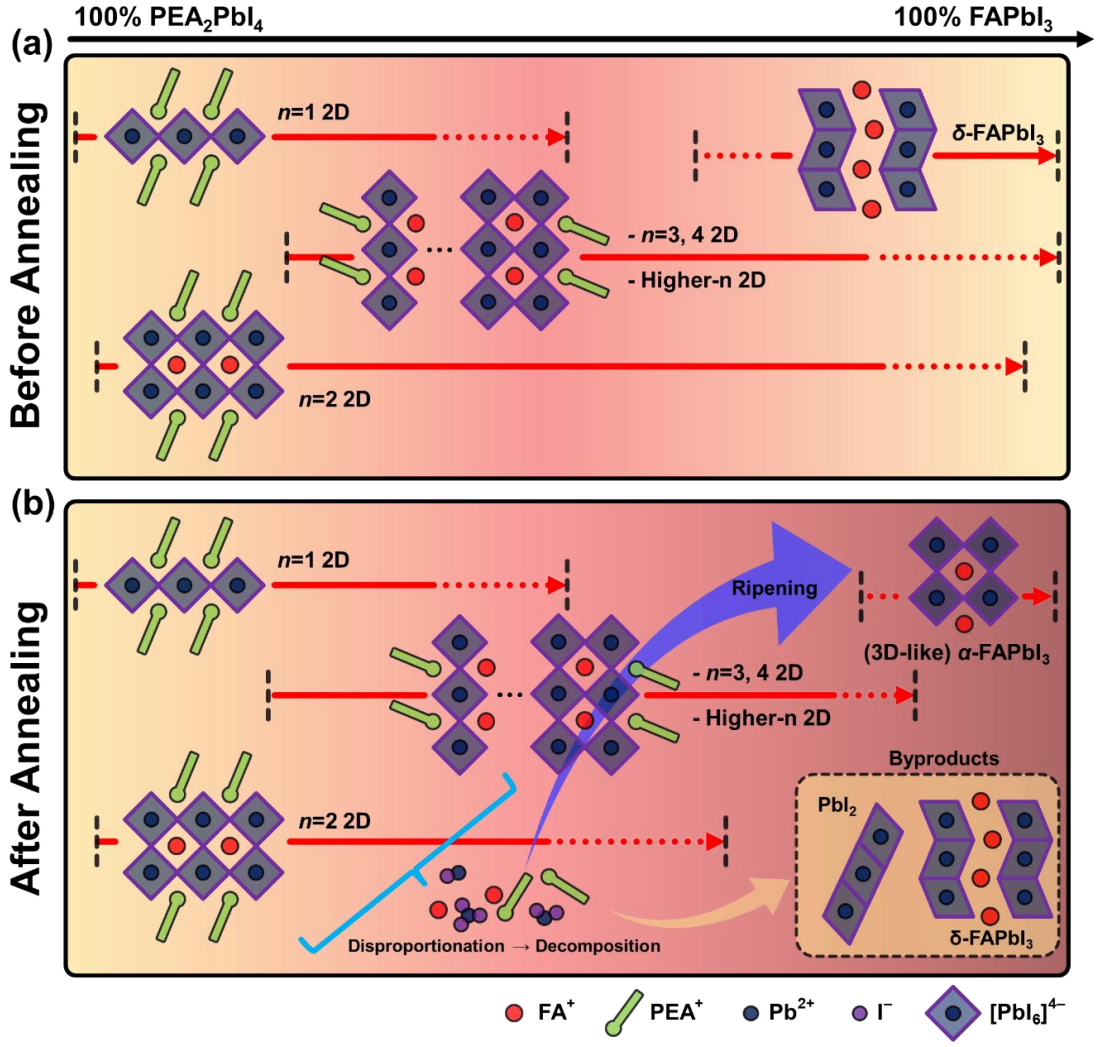


**Figure 4.** Schematic of phase distribution and growth behaviors in PEA-FA quasi-2D MHP film system in a 2D:3D compositional space: (a) before and (b) after annealing. The initial phase distributions are defined at the early-stage phase growth process, as seen in microcrystal system. At high 3D ratios, thermodynamically stable δ-$FAPbI_3$ emerges. By annealing the films, higher-*n* and 3D-like phases are formed at the expense of intermediate *n*=2-4 2D phases via

disproportionation, which also leaves the unwanted $PbI_2$ byproduct.

**Influence of solvent on the phase distribution of quasi-2D MHP**

Solvents play a crucial role in shaping the surface morphology and crystallinity of the resulting MHP films due to their interaction with the precursor solutes.[30-32, 36] Hence, we increased the concentration of MHP precursors to the nominal level for optoelectronic device fabrication and studied the impact of solvent on the phase formation in quasi-2D MHP films (**Figure S18**). For films with 28% 3D ratio, along with the growth of the *n*=1 phase, higher-*n* phases emerge by using more coordinative solvents in the order of GBL < DMF < DMSO (**Figure 5a-c and S19**). The emission from the *n*=1 phase became stronger with increasing Lewis basicity of the solvent (DMSO), in agreement with the trend of growing *n*=1 2D diffraction peak (**Figure S20**). These observations suggest that the disproportionation of the intermediate-*n* phases (particularly *n*=2 phase in this case) is promoted by the coordinative solvents. This has been explained by the increase of nucleation barrier of quasi-2D phases, collectively attributed to the formation of $PbI_2$-solvent adduct and strong spacer-solvent interaction.[40] The polar nature of PEA cation, with a dipole moment of ~14.0 Debye results in strong hydrogen bond with the Lewis base DMSO, inhibiting the 2D phase formation.[40, 41] In contrast, FA has a weak polarity (dipole moment of 0.25 Debye) and therefore the nucleation of 3D phase can be relatively feasible.[42] We collected absorption spectra of 2D and 3D precursor solutions to assess the iodoplumbate formation in the solution phase (**Figure S21**). Indeed, with increasing coordinative character of the solvent, notable imbalance in ionic forms between the 2D and 3D precursors is observed,[31] with the 3D precursor exhibiting more disintegrated forms than the 2D precursor. This results in the broader phase distributions with higher-*n* phases in PL spectra.

At 3D ratios up to 67%, a preferential product i.e., the *n*=2 phase, appears along with a 3D-like phase. At a 3D ratio of 98%, only the single peak of α-$FAPbI_3$ is observed in the films,

regardless of the solvent used, with superior crystallinity compared to pure 3D MHP (sharper XRD peak, **Figure S20**). Particularly, the films produced using the DMF and DMF:DMSO solvent systems show large and smooth MHP grains as seen by scanning electron microscopy (**Figure S22**), showing notable difference with those of pure 3D films. However, the overall surface morphology of the 98% MHP film produced using only DMF is poor, suggesting that the solvent is not compatible for making films with high 3D compositional ratios. The addition of DMSO improves the morphology. We hypothesize that the difference in solute-solvent interaction between 2D and 3D solutions is associated with these results (**Figure S21**). The heterogeneous solvation of precursor ions in different solvents would cause different nucleation kinetics in 2D and 3D phases,[40] where the larger difference (in this case, DMF) could infer the kinetic imbalance and subsequently result in the irregular morphology. For DMF:DMSO mixed solvent system, although there is still an imbalance of precursor solvation, the strong hydrogen bonding between the spacer and DMSO can inhibit the 2D phase growth and promote the selective crystallization and coarsening of 3D phases.[40] As a result, this can renders larger 3D MHP grains,[43] whereas the residual 2D precursors smoothen and passivate the 3D grain surfaces – analogous to the observations in 3D MHPs incorporating alkylammonium salts.[43, 44]

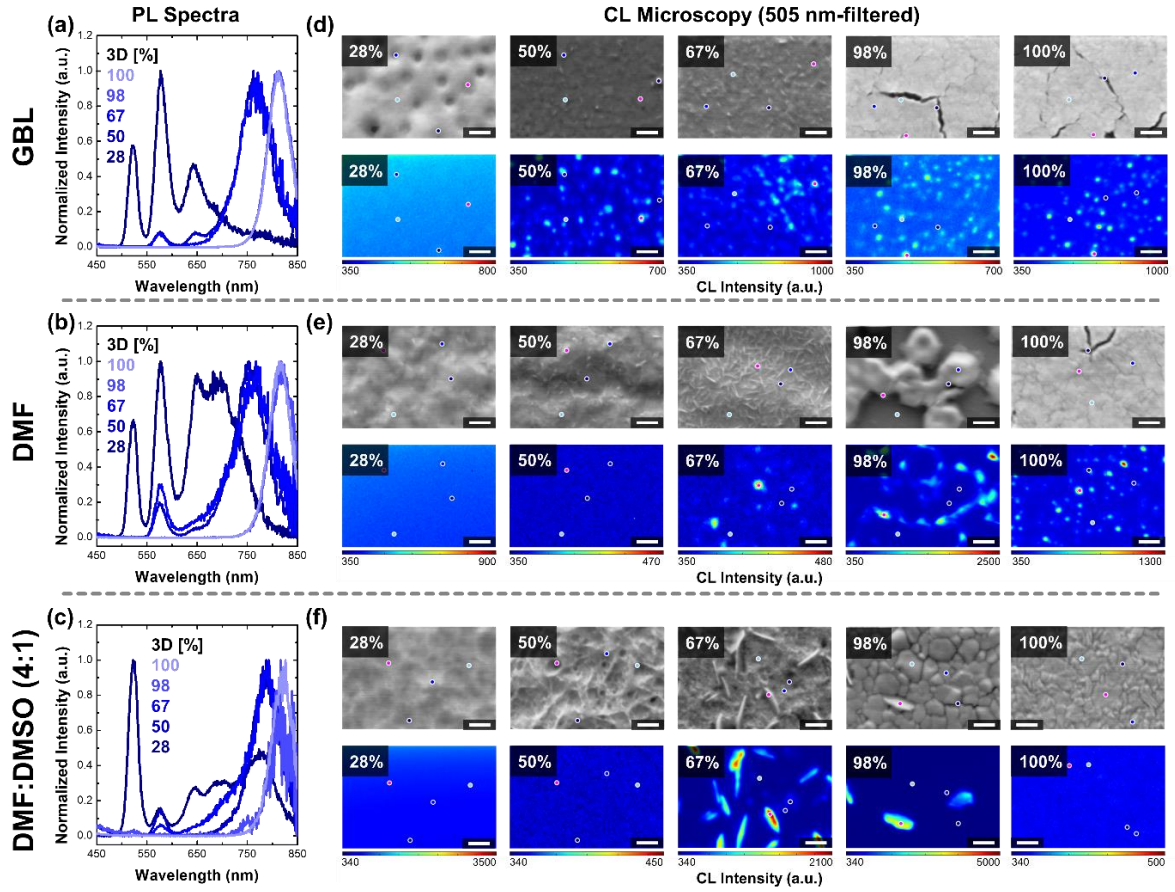


**Figure 4.** (a-c) PL spectra, (d-f) SEM and 505 nm-filtered CL maps (assigned to $PbI_2$) for the quasi-2D MHPs films with different solvent systems. All films were prepared by annealing the spin-casted substrates at 150 $^oC$ for 20 min (Scale bar: 1 μm). Four local spots are chosen and color-marked in the map, where the corresponding CL spectra are shown in **Figure S23**.

From the CL analysis, the presence of local $PbI_2$ crystallites (505 nm CL) in the films is again observed (**Figure 4d-f** and **S23**), with larger sizes seen when DMSO is added in the solvent mixture. While DMSO can make $PbI_2$-DMSO adducts, it can strongly coordinate with PEA cation via hydrogen bonding inhibiting the 2D phase growth.[40] After annealing, the residual adducts, after consuming all FA cations to form $FAPbI_3$ first, could be left. While some of the PEA spacers are used to render smooth 3D MHP grains,[44] the 2D precursor adducts are subsequently transform into large $PbI_2$ aggregates or PEA-poor, defective 2D phases that readily undergo lattice disproportionation. Relatively weaker coordination of DMF could be

responsible for the smaller size of $PbI_2$ crystallites. Meanwhile, the poor surface morphology particularly at 98% 3D ratio could also lead to extrusion of $PbI_2$ alongside the grain exteriors.

A strong 745 nm CL band, which is not detected in photoluminescence analysis, is also observed in films with high 3D ratios (98% and 100%), particularly at grain boundaries or wrinkled surface structures (**Figure S24**). This is attributed to the CL emission from the photoinactive δ-$FAPbI_3$, rather than other low-dimensional $FAPbI_3$ polymorphs,[45, 46] as no significant XRD peaks of the latter are observed. We note that this CL band becomes stronger with increasing the coordinative character of the solvent, which also involves rougher surface morphology with more amounts of wrinkled structures. We hypothesize that the coarse surface edges at the grain boundary and the microstructures – possibly with larger amounts of surface defects[47] – could readily be transformed to the δ-$FAPbI_3$ phase.

Summarizing, the strong chemical interaction between the solvent and precursors leads to significant changes in surface morphology, microstructures, phase distributions and emergence of secondary phases in the quasi-2D MHP films. The spacer cation, due to its high polarity, strongly interact with solvent, where the chemical interaction is proportional to the coordinative strength of the solvent. The increase of solvent-spacer interaction strength can induce an imbalanced solvation of 2D and 3D components in precursor solutions. Subsequently, this largely complicates the MHP crystallization behaviors associated with the surface morphologies, phase inhomogeneities, local microstructures in the films. Solving such complexities requires multimodal approaches including molecular tailoring of the spacers and solvent engineering. High-throughput exploration of the early-stage phase growth kinetics of quasi-2D MHPs and hyperspectral CL microscopy reveal indispensable features and principles associated with the system, which could not be conventionally observed. In turns, these findings provide crucial insights for optimization and development of the functional quasi-2D

MHP system.

## Conclusion

In summary, the phase growth kinetics of PEA-FA quasi-2D MHPs are systematically explored using an automated experimental workflow based on high-throughput automated synthesis, optical characterization and spectral analysis. Without relying on manual intervention, this allows for efficiently monitoring the early-stage phase growth kinetics of 95 different microcrystal ensembles in a quasi-2D MHP compositional space, which could not be properly observed from the conventional film fabrication protocols.

Experimentally, the most preferentially formed and stable phase is found to be the $n$=2 2D phase, which is irrespective to the disproportionation of kinetically-grown products and prominent in the overall compositional space. Furthermore, the $n \geq 5$ phases emerge with increasing 3D ratio up to 95%, as a result of the restricted growth of 3D-like phase by $n$=2 phase; the stable 3D-like phase can be observed after the $n$=2 phase is depleted (from 96%).[13]

Characterizations of the quasi-2D MHP films reveal that the presence of thermodynamically stable δ-$FAPbI_3$ also hinders the formation of the 3D-like phase. Thermal annealing transforms the non-perovskite phase to photoactive α-$FAPbI_3$, thereby allowing the emergence of the 3D-like phase. However, hyperspectral analysis also revealed the emergence of locally formed $PbI_2$ crystallites, presumably due to thermal-assisted disproportionation; this impurity phase is known to negatively impact MHP functionality[27] but difficult to be identified via conventional analysis such as PL and XRD.[37] Furthermore, it is revealed that the choice of spacer cations and solvent system – due to the strong chemical interaction with each other – crucially impacts the phase distributions, surface morphologies and local phase inhomogeneities, necessitating

judicious considerations of molecular and solvent engineering. These new findings provide crucial insights into the phase distributions and growth kinetics in quasi-2D MHP systems, important for optimizing MHP functionality. Furthermore, the powerfulness of the integrated workflow utilized in this work enables us to accelerate of materials discovery, processing optimization, and comprehensive mechanistic study in other functional systems in future.

**Acknowledgements**

J.Y. and M.A acknowledge support from National Science Foundation (NSF), Award Number No. 2043205 and Alfred P. Sloan Foundation, award No. FG-2022-18275. The CL microscopy was supported by the Center for Nanophase Materials Sciences (CNMS) user facility, project CNMS2022-A-01171, which is a US Department of Energy, Office of Science User Facility at Oak Ridge National Laboratory.

**References**

1. Min, H.; Lee, D. Y.; Kim, J.; Kim, G.; Lee, K. S.; Kim, J.; Paik, M. J.; Kim, Y. K.; Kim, K. S.; Kim, M. G.; Shin, T. J.; Il Seok, S., Perovskite solar cells with atomically coherent interlayers on SnO2 electrodes. *Nature* **2021,** *598* (7881), 444-450.
2. Hassan, Y.; Park, J. H.; Crawford, M. L.; Sadhanala, A.; Lee, J.; Sadighian, J. C.; Mosconi, E.; Shivanna, R.; Radicchi, E.; Jeong, M.; Yang, C.; Choi, H.; Park, S. H.; Song, M. H.; De Angelis, F.; Wong, C. Y.; Friend, R. H.; Lee, B. R.; Snaith, H. J., Ligand-engineered bandgap stability in mixed-halide perovskite LEDs. *Nature* **2021,** *591* (7848), 72-77.
3. Ma, D.; Lin, K.; Dong, Y.; Choubisa, H.; Proppe, A. H.; Wu, D.; Wang, Y. K.; Chen, B.; Li, P.; Fan, J. Z.; Yuan, F.; Johnston, A.; Liu, Y.; Kang, Y.; Lu, Z. H.; Wei, Z.; Sargent, E. H., Distribution control enables efficient reduced-dimensional perovskite LEDs. *Nature* **2021,** *599* (7886), 594-598.
4. Boyd, C. C.; Cheacharoen, R.; Leijtens, T.; McGehee, M. D., Understanding

Degradation Mechanisms and Improving Stability of Perovskite Photovoltaics. *Chem Rev* **2019,** *119* (5), 3418-3451.

5. Jeong, J.; Kim, M.; Seo, J.; Lu, H.; Ahlawat, P.; Mishra, A.; Yang, Y.; Hope, M. A.; Eickemeyer, F. T.; Kim, M.; Yoon, Y. J.; Choi, I. W.; Darwich, B. P.; Choi, S. J.; Jo, Y.; Lee, J. H.; Walker, B.; Zakeeruddin, S. M.; Emsley, L.; Rothlisberger, U.; Hagfeldt, A.; Kim, D. S.; Gratzel, M.; Kim, J. Y., Pseudo-halide anion engineering for $\alpha$-$FAPbI_3$ perovskite solar cells. *Nature* **2021,** *592* (7854), 381-385.

6. Blancon, J. C.; Even, J.; Stoumpos, C. C.; Kanatzidis, M. G.; Mohite, A. D., Semiconductor physics of organic-inorganic 2D halide perovskites. *Nature Nanotechnology* **2020,** *15* (12), 969-985.

7. Soe, C. M. M.; Nagabhushana, G. P.; Shivaramaiah, R.; Tsai, H. H.; Nie, W. Y.; Blancon, J. C.; Melkonyan, F.; Cao, D. H.; Traore, B.; Pedesseau, L.; Kepenekian, M.; Katan, C.; Even, J.; Marks, T. J.; Navrotsky, A.; Mohite, A. D.; Stoumpos, C. C.; Kanatzidis, M. G., Structural and thermodynamic limits of layer thickness in 2D halide perovskites. *P Natl Acad Sci USA* **2019,** *116* (1), 58-66.

8. Li, X. T.; Hoffman, J. M.; Kanatzidis, M. G., The 2D Halide Perovskite Rulebook: How the Spacer Influences Everything from the Structure to Optoelectronic Device Efficiency. *Chemical Reviews* **2021,** *121* (4), 2230-2291.

9. Gan, X.; Chen, W.; Liu, C.; Zhang, J.; Di, Y.; Yu, L.; Dong, L.; Jia, B.; Wen, X., Energy Funneling in Quasi-2D Ruddlesden–Popper Perovskites: Charge Transfer versus Resonant Energy Transfer. *Adv Photonics Res* **2022,** *3*, 2100283.

10. Yuan, M.; Quan, L. N.; Comin, R.; Walters, G.; Sabatini, R.; Voznyy, O.; Hoogland, S.; Zhao, Y.; Beauregard, E. M.; Kanjanaboos, P.; Lu, Z.; Kim, D. H.; Sargent, E. H., Perovskite energy funnels for efficient light-emitting diodes. *Nat Nanotechnol* **2016,** *11* (10), 872-877.

11. Quan, L. N.; Zhao, Y.; Garcia de Arquer, F. P.; Sabatini, R.; Walters, G.; Voznyy, O.; Comin, R.; Li, Y.; Fan, J. Z.; Tan, H.; Pan, J.; Yuan, M.; Bakr, O. M.; Lu, Z.; Kim, D. H.; Sargent, E. H., Tailoring the Energy Landscape in Quasi-2D Halide Perovskites Enables Efficient Green-Light Emission. *Nano Lett* **2017,** *17* (6), 3701-3709.

12. Quan, L.; Ma, D. X.; Zhao, Y. B.; Voznyy, O.; Yuan, H. F.; Bladt, E.; Pan, J.; de Arquer, F. P. G.; Sabatini, R.; Piontkowski, Z.; Emwas, A. H.; Todorovic, P.; Quintero-Bermudez, R.; Walters, G.; Fan, J. Z.; Liu, M. X.; Tan, H. R.; Saidaminov, M. I.; Gao, L.; Li, Y. Y.; Anjum, D. H.; Wei, N. N.; Tang, J.; McCamant, D. W.; Roeffaers, M. B. J.; Bals, S.; Hofkens, J.; Bakr, O. M.; Lu, Z. H.; Sargent, E. H., Edge stabilization in reduced-dimensional perovskites. *Nature Communications* **2020,** *11* (1).

13. Lee, J. W.; Dai, Z.; Han, T. H.; Choi, C.; Chang, S. Y.; Lee, S. J.; De Marco, N.; Zhao, H.; Sun, P.; Huang, Y.; Yang, Y., 2D perovskite stabilized phase-pure formamidinium perovskite solar cells. *Nat Commun* **2018,** *9* (1), 3021.
14. Sidhik, S.; Wang, Y.; De Siena, M.; Asadpour, R.; Torma, A. J.; Terlier, T.; Ho, K.; Li, W.; Puthirath, A. B.; Shuai, X.; Agrawal, A.; Traore, B.; Jones, M.; Giridharagopal, R.; Ajayan, P. M.; Strzalka, J.; Ginger, D. S.; Katan, C.; Alam, M. A.; Even, J.; Kanatzidis, M. G.; Mohite, A. D., Deterministic fabrication of 3D/2D perovskite bilayer stacks for durable and efficient solar cells. *Science* **2022,** *377* (6613), 1425-1430.
15. Zhang, F.; Park, S. Y.; Yao, C.; Lu, H.; Dunfield, S. P.; Xiao, C.; Ulicna, S.; Zhao, X.; Du Hill, L.; Chen, X.; Wang, X.; Mundt, L. E.; Stone, K. H.; Schelhas, L. T.; Teeter, G.; Parkin, S.; Ratcliff, E. L.; Loo, Y. L.; Berry, J. J.; Beard, M. C.; Yan, Y.; Larson, B. W.; Zhu, K., Metastable Dion-Jacobson 2D structure enables efficient and stable perovskite solar cells. *Science* **2022,** *375* (6576), 71-76.
16. Sun, C.; Jiang, Y.; Cui, M.; Qiao, L.; Wei, J.; Huang, Y.; Zhang, L.; He, T.; Li, S.; Hsu, H. Y.; Qin, C.; Long, R.; Yuan, M., High-performance large-area quasi-2D perovskite light-emitting diodes. *Nat Commun* **2021,** *12* (1), 2207.
17. Wang, K.; Lin, Z. Y.; Zhang, Z.; Jin, L.; Ma, K.; Coffey, A. H.; Atapattu, H. R.; Gao, Y.; Park, J. Y.; Wei, Z.; Finkenauer, B. P.; Zhu, C.; Meng, X.; Chowdhury, S. N.; Chen, Z.; Terlier, T.; Do, T. H.; Yao, Y.; Graham, K. R.; Boltasseva, A.; Guo, T. F.; Huang, L.; Gao, H.; Savoie, B. M.; Dou, L., Suppressing phase disproportionation in quasi-2D perovskite light-emitting diodes. *Nat Commun* **2023,** *14* (1), 397.
18. Sanchez, S. L.; Yang, J.; Ahmadi, M., Understanding the Ligand-Assisted Reprecipitation of CsPbBr3 Perovskite Nanocrystals via High Throughput Robotic Synthesis Approach. *ChemRixv* **2023**, 10.26434/chemrxiv-2023-bgcg0.
19. Yang, J.; Kalinin, S. V.; Cubuk, E. D.; Ziatdinov, M.; Ahmadi, M., Toward self-organizing low-dimensional organic-inorganic hybrid perovskites_Machine learning-driven co-navigation of chemical and compositional spaces. *MRS Bull* **2023,** *48*.
20. Zhang, J.; Langner, S.; Wu, J.; Kupfer, C.; Luer, L.; Meng, W.; Zhao, B.; Liu, C.; Daum, M.; Osvet, A.; Li, N.; Halik, M.; Stubhan, T.; Zhao, Y.; Hauch, J.; Brabec, C. J., Intercalating-Organic-Cation-Induced Stability Bowing in Quasi-2D Metal-Halide Perovskites. *ACS Energy Letters* **2022,** *7*, 70-77.
21. Zhao, Y.; Hueumaueller, T.; Zhang, J.; Luo, J.; Kasian, O.; Langner, S.; Kupfer, C.; Liu, B.; Zhong, Y.; Elia, J.; Osvet, A.; Wu, J.; Liu, C.; Wan, Z.; Jia, C.; Li, N.; Hauch, J.; Brabec, C. J., A bilayer conducting polymer structure for planar perovskite solar cells with over 1400 hours operational stability at elevated temperatures. *Nat Energy* **2022,** *7*, 144-

152.
22. Higgins, K.; Valleti, S. M.; Ziatdinov, M.; Kalinin, S. V.; Ahmadi, M., Chemical Robotics Enabled Exploration of Stability in Multicomponent Lead Halide Perovskites via Machine Learning. *Acs Energy Letters* **2020,** *5* (11), 3426-3436.
23. Higgins, K.; Ziatdinov, M.; Kalinin, S. V.; Ahmadi, M., High-Throughput Study of Antisolvents on the Stability of Multicomponent Metal Halide Perovskites through Robotics-Based Synthesis and Machine Learning Approaches. *J Am Chem Soc* **2021,** *143* (47), 19945-19955.
24. Long, H.; Peng, X.; Lu, J.; Lin, K.; Xie, L.; Zhang, B.; Ying, L.; Wei, Z., Exciton–phonon interaction in quasi-two dimensional layered (PEA)2(CsPbBr3)n−1PbBr4 perovskite. *Nanoscale* **2019,** *11*, 21867-21871.
25. Pool, V. L.; Dou, B.; Van Campen, D. G.; Klein-Stockert, T. R.; Barnes, F. S.; Shaheen, S. E.; Ahmad, M. I.; van Hest, M. F.; Toney, M. F., Thermal engineering of FAPbI3 perovskite material via radiative thermal annealing and in situ XRD. *Nat Commun* **2017,** *8*, 14075.
26. Milic, J. V.; Zakeeruddin, S. M.; Gratzel, M., Layered Hybrid Formamidinium Lead Iodide Perovskites: Challenges and Opportunities. *Acc Chem Res* **2021,** *54* (12), 2729-2740.
27. Macpherson, S.; Doherty, T. A. S.; Winchester, A. J.; Kosar, S.; Johnstone, D. N.; Chiang, Y. H.; Galkowski, K.; Anaya, M.; Frohna, K.; Iqbal, A. N.; Nagane, S.; Roose, B.; Andaji-Garmaroudi, Z.; Orr, K. W. P.; Parker, J. E.; Midgley, P. A.; Dani, K. M.; Stranks, S. D., Local Nanoscale Phase Impurities are Degradation Sites in Halide Perovskites. *Nature* **2022**.
28. Fu, Y.; Wu, T.; Wang, J.; Zhai, J.; Shearer, M. J.; Zhao, Y.; Hamers, R. J.; Kan, E.; Deng, K.; Zhu, X. Y.; Jin, S., Stabilization of the Metastable Lead Iodide Perovskite Phase via Surface Functionalization. *Nano Lett* **2017,** *17* (7), 4405-4414.
29. Fu, Y., Stabilization of Metastable Halide Perovskite Lattices in the 2D Limit. *Adv Mater* **2022,** *34* (9), e2108556.
30. Radicchi, E.; Mosconi, E.; Elisei, F.; Nunzi, F.; De Angelis, F., Understanding the Solution Chemistry of Lead Halide Perovskites Precursors. *ACS Appl Energy Mater* **2019,** *2*, 3400-3409.
31. Hamill Jr., J. C.; Schwartz, J.; Loo, Y. L., Influence of Solvent Coordination on Hybrid Organic–Inorganic Perovskite Formation. *ACS Energy Letters* **2018,** *3*, 92-97.
32. Yang, J.; Kim, M.; Lee, S.; Yoon, J. W.; Shome, S.; Bertens, K.; Song, H.; Lim, S. G.; Oh, J. T.; Bae, S. Y.; Lee, B. R.; Yi, W.; Sargent, E. H.; Choi, H., Solvent Engineering of

Colloidal Quantum Dot Inks for Scalable Fabrication of Photovoltaics. *ACS Appl Mater Interfaces* **2021,** *13* (31), 36992-37003.
33. Cinquino, M.; Fieramosca, A.; Mastria, R.; Polimeno, L.; Moliterni, A.; Olieric, V.; Matsugaki, N.; Panico, R.; De Giorgi, M.; Gigli, G.; Giannini, C.; Rizzo, A.; Sanvitto, D.; De Marco, L., Managing Growth and Dimensionality of Quasi 2D Perovskite Single-Crystalline Flakes for Tunable Excitons Orientation. *Adv Mater* **2021,** *33* (48), e2102326.
34. Fu, W.; Liu, H.; Shi, X.; Zuo, L.; Li, X.; Jen, A. K. Y., Tailoring the Functionality of Organic Spacer Cations for Efficient and Stable Quasi-2D Perovskite Solar Cells. *Adv Funct Mater* **2019,** *29* (25), 1900221.
35. Hui, W.; Chao, L.; Lu, H.; Xia, F.; Wei, Q.; Su, Z.; Niu, T.; Tao, L.; Du, B.; Li, D.; Wang, Y.; Dong, H.; Zuo, S.; Li, B.; Shi, W.; Ran, X.; Li, P.; Zhang, H.; Wu, Z.; Ran, C.; Song, L.; Xing, G.; Gao, X.; Zhang, J.; Xia, Y.; Chen, Y.; Huang, W., Stabilizing black-phase formamidinium perovskite formation at room temperature and high humidity. *Science* **2021,** *371*, 1359-1364.
36. Jeon, N. J.; Noh, J. H.; Kim, Y. C.; Yang, W. S.; Ryu, S.; Seok, S. I., Solvent engineering for high-performance inorganic-organic hybrid perovskite solar cells. *Nature Materials* **2014,** *13* (9), 897-903.
37. Yang, J.; LaFollette, D. K.; Lawrie, B. J.; Ievlev, A. V.; Liu, Y.; Kelley, K. P.; Kalinin, S. V.; Correa-Baena, J. P.; Ahmadi, M., Understanding the Role of Cesium on Chemical Complexity in Methylammonium-Free Metal Halide Perovskites. *Adv Energy Mater* **2022**, 2202880.
38. Fang, H. H.; Yang, J.; Tao, S.; Adjokatse, S.; Kamminga, M. E.; Ye, J.; Blake, G. R.; Even, J.; Loi, M. A., Unravelling Light-Induced Degradation of Layered Perovskite Crystals and Design of Efficient Encapsulation for Improved Photostability. *Adv Funct Mater* **2018,** *28*, 1800305.
39. An, Q. Z.; Paulus, F.; Becker-Koch, D.; Cho, C.; Sun, Q.; Weu, A.; Bitton, S.; Tessler, N.; Vaynzof, Y., Small grains as recombination hot spots in perovskite solar cells. *Matter* **2021,** *4* (5), 1683-1701.
40. Zhang, X.; Munir, R.; Xu, Z.; Liu, Y.; Tsai, H.; Nie, W.; Li, J.; Niu, T.; Smilgies, D. M.; Kanatzidis, M. G.; Mohite, A. D.; Zhao, K.; Amassian, A.; Liu, S. F., Phase Transition Control for High Performance Ruddlesden-Popper Perovskite Solar Cells. *Adv Mater* **2018,** *30* (21), e1707166.
41. Song, H.; Yang, J.; Jeong, W. H.; Lee, J.; Lee, T. H.; Yoon, J. W.; Lee, H.; Ramadan, A. J.; Oliver, R. D. J.; Cho, S. C.; Lim, S. G.; Jang, J. W.; Yu, Z.; Oh, J. T.; Jung, E. D.; Song, M. H.; Park, S. H.; Durrant, J. R.; Snaith, H. J.; Lee, S. U.; Lee, B. R.;

Choi, H., A Universal Perovskite Nanocrystal Ink for High-Performance Optoelectronic Devices. *Adv Mater* **2022**, e2209486.
42. Zilka, M.; Dudenko, D. V.; Hughes, C. E.; Williams, P. A.; Sturniolo, S.; Franks, W. T.; Pickard, C. J.; Yates, J. R.; Harris, K. D. M.; Brown, S. P., Ab initio random structure searching of organic molecular solids: assessment and validation against experimental data. *Phys Chem Chem Phys* **2017,** *19* (38), 25949-25960.
43. Soe, C. M. M.; Nie, W. Y.; Stoumpos, C. C.; Tsai, H.; Blancon, J. C.; Liu, F. Z.; Even, J.; Marks, T. J.; Mohite, A. D.; Kanatzidis, M. G., Understanding Film Formation Morphology and Orientation in High Member 2D Ruddlesden-Popper Perovskites for High-Efficiency Solar Cells. *Advanced Energy Materials* **2018,** *8* (1).
44. Park, J.; Kim, J.; Yun, H. S.; Paik, M. J.; Noh, E.; Mun, H. J.; Kim, M. G.; Shin, T. J.; Seok, S. I., Controlled growth of perovskite layers with volatile alkylammonium chlorides. *Nature* **2023**.
45. Wang, P.; Chen, X.; Liu, T.; Hou, C. H.; Tian, Y.; Xu, X.; Chen, Z.; Ran, P.; Jiang, T.; Kuan, C. H.; Yan, B.; Yao, J.; Shyue, J. J.; Qiu, J.; Yang, Y. M., Seed-Assisted Growth of Methylammonium-Free Perovskite for Efficient Inverted Perovskite Solar Cells. *Small Methods* **2022,** *6* (5), e2200048.
46. Ma, F.; Li, J.; Li, W.; Lin, N.; Wang, L.; Qiao, J., Stable $\alpha/\delta$ phase junction of formamidinium lead iodide perovskites for enhanced near-infrared emission. *Chem Sci* **2017,** *8* (1), 800-805.
47. Xue, J.; Wang, R.; Wang, K. L.; Wang, Z. K.; Yavuz, I.; Wang, Y.; Yang, Y.; Gao, X.; Huang, T.; Nuryyeva, S.; Lee, J. W.; Duan, Y.; Liao, L. S.; Kaner, R.; Yang, Y., Crystalline Liquid-like Behavior: Surface-Induced Secondary Grain Growth of Photovoltaic Perovskite Thin Film. *J Am Chem Soc* **2019,** *141* (35), 13948-13953.